International Journal of Fatigue, Volume 33, Issue 11, November 2011, Pages 1417–1425

Size Effects on Residual Stress and Fatigue Crack Growth in Friction Stir Welded 2195-T8 aluminium Part I: Experiments

Yu E Ma[1, 2], P Staron[3] T Fischer[3], P. E. Irving[2]

[1] School of Aeronautics, Northwestern Polytechnical University, China; [2] Damage Tolerance Group, School of Applied Science, Cranfield University, UK; [3] Institute of Materials Research, Geesthacht, Germany

ABSTRACT: Residual stress fields were measured in three different sizes of Compact-Tension (C(T)) and eccentrically loaded single edge notch (ESE(T)) specimens containing transverse or longitudinal welds. The effect of size on residual stress profiles was studied. Fatigue crack growth tests were carried out with cracks growing into or away from the weld line, as well as growing along the weld centre line. Effects of weld residual stresses on fatigue crack growth rates parallel and perpendicular to the friction stir welds were studied. It wan found that compressive residual stresses around the sample notch had significant retarding effects on both crack initiation and crack growth rates for cracks growing towards the weld line. Effects of residual stress on crack growth rates declined with increasing crack length. When cracks grew parallel to the weld line in C(T) samples the crack growth rate was around 20% lower than in parent material.

Keywords: Friction stir weld; Residual stress; Sample size effect; Crack closure; Fatigue crack growth

NOMENCLATURE

a = crack length
K = stress intensity factor
K_{res} = stress intensity factor from residual stress
N = cycle (fatigue load)
da/dN = crack growth rate
E = the Young's modulus (modulus of elasticity)
R_{nom} = applied load R ratio
R_{eff} = R ratio with the presence of residual stress
ΔK_{eff} = the effective stress intensity factor range
S_o = the crack opening stress
$S_{\max}, S_{\min}$ = applied maximum, minimum stress

INTRODUCTION

The effects of residual stresses on fatigue crack growth rates in welded samples have been studied by many researchers in the past 20 years. As residual stress measurement techniques improve more comprehensive knowledge of the form of weld residual stress fields has become more widely appreciated. Models to predict crack growth rates in the presence of residual stresses have been available for some years, but only recently has knowledge of residual stress fields become sufficiently comprehensive to allow quantitative model validation. A particular difficulty is the mixture of different variables contained within a weld which makes it hard to distinguish effects of microstructure and hardness changes within the weld from those due to residual stress. A related question is whether there can be “intrinsic” crack growth resistance within a weld separate from effects of residual stress. The former is something that will be unchanging with sample geometry, the latter will depend on sample geometry and post weld machining as well as on the weld process itself.

In order to quantify residual stress effects in different sample sizes and geometries, in this research samples of C(T) and ESE(T) geometry in 3 sizes were manufactured from plates of 2195-T8 Al-Li alloy containing friction stir welds. The residual stress profiles were measured by the neutron diffraction method before fatigue testing. The weld crack growth rates and crack paths were compared with those found in parent material. Experimental results are reported in Part I; Part II reports on model development to predict growth rates using measured residual stresses based on the K_{res} approach.

Residual stresses and crack growth rates in friction stir welds

Several methods have been used to measure the residual stress distribution in welded plates. These include: synchrotron X-ray scanning [1]; sample slitting [2]; neutron diffraction [3-5]; cut compliance [6-7]; hole drilling [8]; magnetizing stress indication [9], and the contour method [10]. Stress fields measured by all techniques show similar features with a double-peak in longitudinal stress with the maxima in the heat affected zones on each side of the weld line, with a smaller stress in the central weld line (the nugget). Residual stresses are greatest on the tool advancing side of the weld than on the retreating.

Residual stress effects on fatigue crack growth of FSW aluminium have been studied in previous research [5-7; 11-19]. The major conclusions of this work are as follows.

(1) Residual stress is the most important parameter influencing fatigue crack growth rates, with tensile stresses increasing crack growth rates, and compressive stresses decreasing them [5-7, 11-19].

(2) Residual stresses are not the only significant influence; microstructure of the FSW nugget region together with its local toughness and ductility play a role for cracks in the nugget [6,7].

(3) Redistribution and relaxation of residual stress as the crack grows has important effects on crack growth [5].

Despite substantial work in definition of the influencing parameters there are still relatively few examples of work where crack growth rates and residual stresses have both been measured and the results of model predictions can be validated across a range of goeometries and orientations of the crack and weld [13-16]. This is particularly true for sample size effects, where sample size will influence residual stresses which in turn will influence crack growth rates.

EXPERIMENTAL PROCEDURES

Parent material properties

The composition and mechanical properties of 2195-T8 parent material are shown in Table 1 and Table 2 [20]. This “third generation” Al-Li alloy, 2195-T8 has a greater Cu/Li ratio than the second generation alloys 2090 and 2091 [21]. Compared with 2024 (0.2% proof strength of 350 MPa and UTS of 490 MPa), the mechanical properties of 2195 are improved significantly, with 0.2% proof strength of 580 MPa and UTS of 615 MPa. Young’s modulus is increased to 79 GPa. Plates of this alloy have an elongated grain structure due to the rolling process. This is shown in Fig.1. The grain shape is highly anisotropic being about 1.5 mm long and 1.4 μm thick when sectioned in the L-ST plane.

Sample manufacture

A series of 12.7 mm thick 2195-T8 Al-Li alloy plates 1 m long were friction stir welded. All weld directions were parallel to the rolling direction. From these 1 m welded plates, C(T) and ESE(T) samples of the sizes shown in Table 3 were machined. In this process the sample thickness was reduced to 8 mm. In order to reduce distortion arising during the skimming operation, the thickness was reduced by removing 0.1 mm alternately from the top and bottom surfaces. Fig. 2 shows the sample geometries and crack orientations with respect to the weld line. Cracks were parallel to the weld in C(T) samples and perpendicular to the weld for ESE(T) samples, C(T) geometries were chosen for cracks parallel to the weld as excessively large ESE(T) sample dimensions would be required for a transverse crack which retained significant residual stresses parallel to the weld.

A macro picture of the cross-section of the weld zone is shown in Fig.3a. The microstructure of the weld was observed on specimens after polishing and etching in Keller's reagent; this is shown in Fig. 3b. As expected, the nugget has a fine equiaxed recrystallized structure with grain size about 10 μm, in contrast to the elongated grains of the parent material shown in Fig.1.

The Vickers microhardness profiles measured at top, bottom and mid-thickness across the weld are shown in Fig.4. In the weld zone, the microhardness is less than the parent material (~200HV) and almost constant at around 130HV. Microhardness profiles have a "W" shaped distribution typical of many friction stir welds in precipitation hardening aluminium alloys [5, 6]. Microhardness had a difference from top, mid-thickness to bottom in the weld zone (nugget) from about 140 HV to 135 HV to 122 HV. The two microhardness minima at the edge of the nugget are located in

the thermo mechanical affected zone. The top side has a wider nugget zone than the bottom side, which leads to the smaller HV values of the top side, see Fig. 4.

Since all samples were machined from identical 12.7 mm welded plates, the microstructure and hardness of welds in all samples will be the same, but samples are expected to have different residual stress distributions and profiles arising from different sample sizes.

Fatigue test procedure

Fatigue tests were performed on all samples using either a 30 kN or a 100 kN servo hydraulic test machine equipped with digital control. Procedures described in ASTM E647 were followed. Tests were performed at R=0.1 and R=0.6 with a cycle frequency of 10 Hz. The applied load ranges were 3.8 kN, 5.7 kN and 8.34 kN for the 3 ESE(T) samples, and 4.38 kN, 5.80 kN and 8.48 kN for the CT samples. Stress intensity factors for all specimens were calculated using the expressions recommended in ASTM E647. The electric potential method [22] was used to monitor crack growth. The crack length measurement system was controlled by Labview 8.5 software, and was accurate to ±0.1 mm.

Measurement of residual stresses

In order to investigate the influence of the sample dimensions on residual stress profiles, 3 ESE(T) and 3 C(T) test samples of the sizes shown in Table 3 were subjected to neutron diffraction. Readings were taken at intervals of 3 mm along a line along or across the weld line. Line locations and orientations are shown in Fig. 5 for the two sample geometries. Residual stresses parallel with the weld direction are termed X direction stresses; while those perpendicular to the weld line are called Y direction stresses.

The residual stress measurements were carried out using the neutron diffractometer ARES-2 at HZG[3, 23]. Neutrons of 0.164 nm wavelength were chosen with a silicon (311) monochromator. Each specimen was scanned three times to measure the three independent strains in longitudinal (LD), normal (ND), and transverse (TD) directions. The gauge volume was defined by primary and secondary Cd slits with a height of 6 mm (ND/TD) or 3 mm (LD) and a width of 3 mm. These slits form a gauge volume with a nominal size of 3 mm × 3 mm × 6 mm (ND/TD) and 3 mm × 3 mm × 3 mm (LD). The gauge volume was placed at the middle of the sheet thickness. A gas filled DENEX area detector was used to measure the peak shift of the aluminium (311) reflection at an angle of 84.4°. The (311) reflection is recommended because of its isotropic characteristics providing access to the macro stresses. The measured diffraction peaks were fitted with a Gaussian function. The approximation of a biaxial stress state was made for the calculation of stress-free lattice parameters and stresses. In general, diffraction elastic constants for the specific set of lattice planes used for the diffraction measurement have to be used for calculating stresses from the measured strains. However, the elastic anisotropy of aluminium is small and thus the bulk values of Young's modulus and Poisson's ratio were used. For each ESE(T) sample, a single scan was performed, perpendicular to the weld line at the location of the edge notch on the sample centre line, as shown in Fig.5(a). The scan line end was placed at the notch tip, and the first measurement location was 3 mm from the tip. The distance between successive measuring points was also 3 mm. For CT samples two scans were performed to evaluate the residual stress state, as shown in Fig.5 (b). The first scan line was placed perpendicular to the weld line half way between the notch tip and edge of the specimen. The second line was parallel to the weld on the weld centreline. The first measurement point on the second line was 3 mm from the notch

tip. For the first scan the distance between measurement points was 3 mm; for the second line it was 5 mm.

RESULTS

Residual stresses in ESE(T) samples; weld parallel to sample long axis

Residual stress profiles for three sizes of ESE(T) samples (148x40 mm, 185x50 mm and 370x100 mm) are shown in Fig.6. In Fig.6 (a), X-direction stresses parallel to the weld direction have a double peak tensile residual stress field of similar form in all three specimens. The maximum tensile residual stress parallel to the weld ranged from 120 MPa, for the largest sample to 47 MPa, in the smallest. Remote from the weld line at the notch tip, the minimum stress value varied from about -130 MPa to -20 MPa compression for the largest and smallest samples.

In Fig.6 (b), the stresses perpendicular to weld (Y-direction) are shown. The Y direction stresses did not change over the scan line as much as in the X direction, and was roughly zero (±10 MPa) at the weld line. At the notch tip, the residual Y stresses were -50 MPa compression in the biggest sample and -20 MPa in the other two samples. Around the notch tip, residual stresses were always negative for all three sizes, both parallel and perpendicular to the weld.

Residual stresses in C(T) samples; -welds perpendicular to sample loading direction and cracks parallel to the weld

Fig.7 shows the residual stress profiles in three size C(T) test samples (84x87.5, 120x125 and 240x250). Fig.7 (a) shows residual stress profiles for stresses parallel to the weld line on a line across the sample centre (scan line 1). All three C(T) sample

sizes show a double peak in stress, similar to that found in ESE(T) samples. The maximum residual stress parallel to the weld varied from 110 MPa for the largest sample to 95 MPa for the intermediate to 82 MPa, for the smallest. Residual stresses perpendicular to the weld at this location along the weld line were small (as in the ESET samples), with a mean value of about 25 MPa tension; sample size having little systematic effect. This is shown in Fig.7 (b).

Figs.8 a and b shows how residual stress measured along the weld centreline changes with distance across the CT sample width. Near the notch tip residual stresses are compressive but change rapidly into tension with distance away from the notch achieving a maximum of 45 MPa before reducing again as the far sample edge is approached. On the weld centreline stresses parallel and perpendicular to the weld were of similar size, with stresses perpendicular to the weld often greater than those parallel in all C(T) samples. Around the notch tip, residual stresses both perpendicular and parallel to the weld were compressive. Fig. 7b shows that stresses perpendicular to the weld change little with distance away from the weld centreline up to a distance of 10 mm from the line. Outside the weld TAZ they reduce with increasing distance to near zero.

Fatigue crack growth testing

ESE(T) samples

Data from the tests on the smallest 40 mm wide sample at R ratios of 0.1 and 0.6 are compared with those from parent material in Fig.9. Fatigue crack growth rates in the welded sample were 10-20 times smaller than parent material growth rates at R=0.1. For R=0.6, crack growth rates in the welded sample were almost the same as those of the parent material, except at the highest values of ΔK where the parent material exhibited slightly faster growth rates. In the parent material there was a limited effect

(about a factor of 2 on da/dN) of R at ΔK values up to 10 MPa $m^{-1/2}$. Above this growth rates at R = 0.6 became much greater than those at R = 0.1.

It was not possible to initiate fatigue cracks at the notches of the two largest welded samples at R=0.1, even after prolonged fatigue cycling. However, cracks were successfully initiated at R=0.6 in the two large samples after only 10^4 cycles. Crack growth rates at R = 0.6 measured on all three samples are shown in Fig. 10a in comparison with parent material for R = 0.6. For samples 370 x 100 and 185 x 50, the crack growth rates are smaller than parent material growth rates by a factor of 4 and 2 at the same ΔK value of 10.5 MPa√m. Crack growth rate in 185 x 50 and 370 x100 samples had an anomalous change in gradient in the curve of da/dN versus ΔK at ΔK values of 12.0-16.0 MPa√m and from 13.0-18.0 MPa√m at crack growth rates around 4.5×10^{-7} m/cycle. Figure 10b shows a plot of growth rate vs. crack length as measured from the weld centreline and demonstrates that these anomalies occurred at different distances (between 6 and 10 mm and 10 to 14 mm from the weld line in the two sample sizes. This suggests that their occurrence does not correspond to a particular microstructure feature at a fixed distance from the weld line.

Fatigue crack growth rates in C(T) samples

In these samples the fatigue crack grew parallel to the weld, initially in the weld centre line. Figure 11 shows fatigue crack growth rates for R=0.1 for the three sizes of sample. Also shown are growth rates in parent plate at the same R ratio. All fatigue crack growth rates in welded samples were slower than those in the parent plate. The differences are greatest at smallest ΔK values corresponding to the smallest crack lengths, and were least or negligible at $\Delta K > 20$MPa $m^{1/2}$. For the sample 250x240 mm, crack growth rate was 30 times less than parent material at ΔK=13MPa√m, decreasing to less than a factor of 2 difference at $\Delta K > 20$MPa $m^{1/2}$. Cracks in smaller samples

grew faster but always slower than in the parent plate. Differences between the 3 welded samples and parent plate were negligible as the ΔK value approached 30MPa $m^{1/2}$.

Crack path changes

ESE(T) Fracture surface

The fatigue crack paths of all specimens were studied after failure. Fig.12 shows the fracture surface of the 185 X 50 mm ESET sample. Different zones can be seen along the crack growth direction. From the notch root, the crack grew smoothly in the parent material before growing into the weld. The crack then grew into the thermo mechanical affected zone (TMAZ). When the plates were welded, the weld top side has a wider nugget and TMAZ than the bottom side because the weld tool shoulder is on the top. The weld zone is around 25 mm wide on the top, and around 12 mm on the bottom. When the crack grows into the recrystallized nugget, the growth rate becomes slower than in other zone, shown in Fig.10. For 370x100 and 185x50 samples, there was a flat form in the curve of da/dN versus distance from the weld centreline (Fig. 10b). The nugget microstructure was believed to play the main role in this behaviour.. For the smallest sample 148x40, the notch root was close to the nugget and the crack was initiated there and grew smoothly throughout. All specimens broke when the cracks grew out of the far edge of weld. This may be a consequence of reduced fracture toughness in the TMAZ compared with the nugget region; sample failure resulting when the crack tip entered this zone.

C(T) Fracture surfaces

Differences in fracture surface morphology were observed between the parent plate fracture surface and that produced by the fatigue crack propagating on the weld line. This is shown in Fig.13. For parent material, the fracture surface is very smooth along the crack growth direction, shown in Fig 13(a), while for welded samples, clear "wave" lines perpendicular to the direction of crack growth and are present in the fracture surface along crack growth direction. These marks reflect the topography of the original friction stir weld surface and may be coincident with successive positions of the rotating tool perimeter as it advances through the material.

Cracks for all CT samples were observed to deviate away from the weld line and nugget region into the thermal mechanically affected zone (TMAZ) on the advancing side, and then grew in the TMAZ until sample failure. Crack location in sample 125x120 is shown in Fig.14. The crack was initiated at the notch in the middle of the weld nugget, grew in the nugget about 8.0 mm; then started to deviate from the weld centreline at the angle of 15° until it entered the thermal mechanically affected zone. The deviation back towards the nugget illustrated in fig 14 marks the crack length at final sample failure in a single load application.

DISCUSSION

Residual stresses

Stress field topography

The two sample geometries with 3 sample sizes allow a comprehensive picture to be developed of changes in weld residual stress produced by changes in sample size.

In all samples stresses parallel to the weld line follow the previously reported [1-10] generic form. Tensile stress maxima occur 10 mm on either side of the weld centre,

with a subsidiary minimum in the weld centre. At distance >10-20 mm from the weld line stresses parallel to the weld move into compression. Interestingly the presence of the notch on one side of the weld moves the stresses in adjacent material further into compression than in the corresponding volume on the opposite side. For example in 100 mm wide ESE(T); stresses of -130 MPa 2 mm from the notch occur as opposed to stresses of -60 MPa at an equal distance on the other side of the weld (shown in Fig.6 (a)). This effect occurs at distances of 4 to 5 mm from the notch root and is therefore not exclusively due to the stress concentration at the notch root, but is due instead to local stress redistribution on removal of material from the notch volume. The same effect is seen in C(T) samples on scan line 2 in Figure 8a.

Residual stresses perpendicular to the weld direction are negligible within the weld itself in ESE(T) samples (figure 6b), but in the largest 100 mm wide sample near the notch in parent plate approach -50 MPa in compression and -10 to -20 MPa at this location in the two smaller samples. In CT samples stresses perpendicular to the weld line are larger, between 40-50 MPa tension (figure 7b). As cracks are growing parallel to the weld in C(T) samples, stresses perpendicular to the weld will influence crack growth. As crack growth begins on the weld centreline, stresses perpendicular to the weld are relevant. These are shown in figure 8b. Again it can be seen that the stresses near the notch root are always compressive moving into tension within 10 mm from the notch, reaching a maximum toward the centre of each sample before declining into compression as the sample rear face is approached. Residual stress maxima perpendicular to the weld are generally smaller than those parallel to the weld in both C(T) and ESE(T) geometries, but on the weld centreline itself are often of similar size leading to an equibiaxial tensile field within which the crack grows.

For all CT samples, residual stress along the weld is much higher than perpendicular to the weld. Parallel to the weld residual stress in the advancing side is about 40 MPa higher than in the retreating side for 87.5x84 and 125x120 samples (shown in Fig.7 (a)). When the crack grew in the weld centreline, the larger residual stresses on the advancing side led the crack to deviate from the weld centreline to the advancing side, (shown in Fig.14).

Effect of sample size on residual stress maxima

Figure 15 shows how the maximum residual tensile stress parallel to the weld direction in each sample changes with weld length and sample width. Also shown are estimated positions of contours of equal stress consistent with the measured stress values and with the constraint that stress must reduce to zero sample width and zero weld length. In Fig.15 the contour line positions other than at the measurement points are obviously estimates. Their positions are consistent with the data points shown given the two constraints of residual stresses tending to zero along both axes and that the contour lines must not cross each other, there is little flexibility possible in the position of the contours within the set of geometries covered by the 6 samples.

As expected the contours of equal maximum stress are roughly parallel to the sample length and width axes, with largest maxima being achieved at regions of greatest width and length. Fig. 15 shows that to achieve the largest residual stresses sample width must exceed approximately 200 mm, and length should exceed 350 mm. It may be that at still larger sizes greater residual stress maxima might be recorded; at smaller sizes than this, residual stresses are changing rapidly with changes in sample size.

Effects of residual stress on fatigue crack growth rates

Both initiation of cracks at notches and their growth through the sample were influenced by residual stresses. Around the notch tip for both C(T) and ESE(T)

samples, residual stress perpendicular and parallel to weld were always compressive. This explains why it was very difficult to initiate the crack when testing at the small mean stress of R=0.1, especially for ESE(T) samples which have the largest compressive residual stresses. Although at R = 0.1 the nominal applied cyclic stress range is tensile, the residual stresses will move the entire stress range into compression. Thus the ΔK_{eff} of any developing cracks will be zero. At the R ratio of 0.6, the applied mean tension stress will be greater than at R=0.1. Addition of the same compressive residual stress now results in the stress cycle being at least partially in tension, ΔK_{eff} will be non zero and crack growth can occur. For 2 of the ESE(T) samples at R=0.6, the crack growth rate tended to remain at around $4.5x10^{-7}$ m/cycle as the crack approached the weld centre; this may be because of the grain size in the thermal affected zone and nugget being different from parent material. When the crack grew out of the nugget, the crack grew faster in the TMAZ, prior to final fracture.

The crack growth rates in C(T) samples where the crack started on the weld centreline (Fig. 11) show a smooth increase of growth rate with ΔK in all three sample sizes and do not have the discontinuities and irregularities found in the crack growth across the weld in ESE(T) samples shown in figure 10. This is despite the observation that the crack slowly deviates out of the weld centreline and into the TMAZ as the test progresses. It may be that this more gradual transition in microstructure than found for the crack crossing the weld in the ESE(T) samples, means that sudden changes in growth rate are not observed. Fig. 11 shows that at long crack lengths (ΔK values of > 20 MPa $m^{1/2}$) the growth rates of the two smallest CT samples are similar, growth rates being slower than in the parent plate grain structure by a factor of 2. It will be shown in Paper II that at these crack lengths initial residual stresses have redistributed

and are small, Hence any differences in growth rate observed can be ascribed to microstructural or strength effects rather than ones of residual stress.

Crack growth rates in CT samples at shorter crack lengths, before any appreciable stress redistribution has occurred due to crack growth, will be influenced additionally by the local residual stresses perpendicular to the weld line. These are shown in Fig. 8b and are compressive at the notch root, retarding the crack, and moving into tension with increasing crack length.

The position of the TAZ can be seen on the ESE(T) sample fracture surface shown in Fig.12,. The top side has a wider weld zone than bottom side, which means the crack will grow into thermal affected zone first at top side, while crack is still growing in parent material in the bottom. The peculiar fracture surface shown in fig. 12 will result from this process.

In part II of this work, K_{res} arising from the residual stresses in all the samples will be calculated using the measured residual stress data, and crack growth rate will be modelled using the ΔK_{eff} approach.

CONCLUSIONS

(1) Residual stress fields in notched C(T) and ESE(T) samples of 2195-T8 aluminium containing friction stir welds have a double peak tensile stress distribution of up to 120 MPa parallel to weld direction, with reduced stress on the weld centreline. Residual stresses perpendicular to the weld are generally smaller than those parallel to the weld. Around the notch tips, both stress components are compressive with stresses approaching -120 MPa in the largest samples.

(2) Samples with weld line lengths greater than 350 mm and sample widths greater than 200 mm are required to achieve the largest measured residual stresses. Samples smaller than this have reduced peak values of stress.

(3) For ESE(T) samples crack growth rate in the smallest 148x40 mm sample is 10 times smaller than that of parent material at R=0.1. At R=0.6, crack growth rates in 370x100 and 185x50 are reduced by factors of 4 and 2 compared with parent material. The crack growth rate at R=0.6 of the smallest sample is similar to parent plate. These growth rate differences are associated with residual stress field changes arising from the different sample sizes.

(4) In C(T) samples, crack growth rates were 5-10 times slower than in the parent material; this difference was greatly reduced at longer crack lengths.

(5) Changes in macroscopic appearance of the fracture surfaces were observed in ESE(T) samples. These corresponded to the different weld zones crossed by the crack of parent material, thermal affected zone (TAZ), and nugget. For C(T) samples the crack grew parallel to the weld with the notch in the nugget; with increased crack length cracks deviated from nugget into TAZ, then grew in it until sample failure.

Acknowledgement The project is funded by the European Commission through a Framework Programme 6 project entitled “cost effective integral structures (COINS)” under contract number AST5-CT-2006-030825. Grateful thanks to Rob Maziarz, Airbus UK for performing the friction stir welding.

REFERENCES

[1] J. Altenkirch, A. Steuwer, M. Peel, D. G. Richards and P. J. Withers (2008). The effect of tensioning and sectioning on residual stresses in aluminium AA7749 friction stir welds. Materials Science and Engineering, 488 (1-2), 16-24.

[2] M.T. Milan, W.W. Bose Filho, J.R. Tarpani et al (2007). Residual stress evaluation of AA2024-T3 friction stir welded joints. Journal of Materials Engineering and Performance, 16(1), 86-92.

[3] P. Staron, M. Kocak, S. Williams, A. Wescott (2004). Residual stress in friction stir-welded Al sheets. Physical B 350, e491-e493.

[4] M.A. Sutton, A.P. Reynolds (2002). A study of residual stresses and microstructure in 2024-T3 Aluminium friction stir but welds. Journal of Engineering Materials and Technology, 124, 215-221.

[5] C.D.M. Liljedahl, J.Brouard, et al (2009). Weld residual stress effects on fatigue crack growth behaviour of aluminium alloy 2024-T351. International Journal of Fatigue, 31, 1081-1088.

[6] G. Pouget, A.P. Reynolds (2008). Residual stress and microstructure effects on fatigue crack growth in AA2050 friction stir welds. International Journal of Fatigue 30, 463–472.

[7] L. Fratini et al. (2009). Fatigue crack growth in 2024-T351 friction stir welded joints. Int J Fatigue 31, 495-500.

[8] Leggatt R.H., et al. Development and experimental validation of the deep hole method for residual stress measurements. J Strain Anal, 1996 ; 31 : 177-86.

[9] Buttle D.J, Scruby C. Residual stresses: measurement using magnetoelastic effects. In : Buschow KHJ, et al., editors. Encyclopedia of materials : science & technology. Elsevier: Oxford, 2001, p. 8173-80.

[10] Prime M. The contour method : simple 2D mapping of residual stresses. In : 6th International conference on residual stress. Oxford: Institute of Materials, 2000.

[11] G. Bussu and P. E. Irving (2003). The role of residual stress and heat affected zone properties on fatigue crack propagation in friction stir welded 2024-T351 aluminium joints. International Journal of Fatigue, 25(1), 77-88.

[12] Hong Seongjin, Kim Sangshik et al (2006). Fatigue crack propagation behaviour of friction stir welded Al-Mg-Si alloy. Scripta Materialia 55, 1007-1010.

[13] Anne-Laure Lafly, Claudio Dalle Donne et al (2006). Role of residual stresses on fatigue crack propagation of FSW 6056-T78 aluminium joints under various technologies. Materials Science Forum Vols. 519-521, 1089-1094.

[14] C.D.M. Liljedahl, O. Zanellato, M.E. Fitzpatrick, J. Lin, L. Edwards. The effect of weld residual stresses and their re-distribution with crack growth during fatigue under constant amplitude loading. International Journal of Fatigue, 32 (2010): 735-743.

[15] Z. Barsoum, I. Barsoum. Residual stress effects on fatigue life of welded structures using LEFM. Engineering Failure Analysis, 16 (2009): 449-467.

[16] C.D.M. Liljedahl, M.E. Fitzpatrick, L. Edwards. Evolution of residual stresses with fatigue crack growth in integral structures with crack retarders. Materials Science and Engineering A, 523 (2009): 152-159.

[17] R. John, K.V. Jata, K. Sadananda (2003). Residual stress effects on near-threshold fatigue crack growth in friction stir welds in aerospace alloys. International Journal of Fatigue, 25, 939-948.

[18] C Dalle Donne, G Biallas, T Ghidini, G Raimbeaux (2000). Effect of weld imperfections and residual stresses on the fatigue crack propagation in friction stir welded joints. In: Proceedings of the second international symposium on friction stir welding, Gothenburg, Sweden; June 2000.
[19] C Dalle Donne, G Raimbeaux (2001). Residual stress effects on fatigue crack propagation in friction stir welds. In: Tenth international conference on fatigue ICF10, Hawaii, USA; 2001.
[20] www.alcanaerospace.com accessed 02042009.
[21] T. Warner. Recently developed aluminium solutions for aerospace applications. Materials Science Forum, 2006 July, Vols. 519-521, 1271-1278.
[22] R.P.Wei, R.L. Brazil (1981). An assessment of A-C and D-C potential systems for monitoring fatigue crack growth. Fatigue crack growth measurement and data analysis, 103-119.
[23] J. dos Santos, GKSS report to COINS project, April 2008.

Tables

Table 1 Chemical composition of 2195-T8 aluminium alloy

element	Si (max)	Fe (max)	Cu	Mn (max)	Mg	Zr	Li	Ag
Wt %	0.12	0.15	3.7-4.3	0.75	0.36	0.08 - 0.16	0.8-1.2	0.25 -0.6

Table 2 Mechanical property of 2195-T8 aluminium alloy

	0.2% proof (MPa)	UTS (MPa)	E (GPa)	Elongation (%)
	580	615	79	9

Table 3 Dimensions of C(T) and ESE(T) Samples

Relationship with weld	Type	Sample size (mm) length x width	W (mm)
Crack parallel to weld	C(T)	84x87.5	70
		120x125	100
		240x250	200
Crack perpendicular to weld	ESE(T)	148x40	40
		185x50	50
		370x100	100

Figure Captions

Figure 1 a & b Microstructure of parent material 2195-T8 Al-Li alloy; L-ST plane

Figure 2 Macro and microstructure of weld zone in 2195-T8 FSW joints; (a) cross section view of weld; (b) microstructure in higher magnification

Figure 3 Vickers microhardness profiles of friction stir weld in at top, bottom and mid-thickness sections across the weld

Figure 4 Schematic diagram showing weld location (a) C(T) and (b) ESE(T) samples

Figure 5 ESE(T) and C(T) samples showing scan lines for measurement of residual stress (a) ESE(T); (b) C(T)

Figure 6 Residual stress profiles in ESE(T) samples (a) Residual stress parallel to weld direction for 3 sizes of ESE(T) samples; (b) Residual stress perpendicular to weld direction in 3 sizes of ESET samples. Shaded area shows extent of weld nugget region.

Figure 7 Residual stress profiles across the weld (1^{st} scan line) in three sizes of C(T) samples, (a) Residual stress parallel to weld direction (b) Residual stress perpendicular to weld direction. Shaded area shows extent of weld nugget region

Figure 8 The effects of sample size on residual stress profiles (2^{nd} scan line) in C(T) samples; (a) Residual stress parallel to weld direction; (b) Residual stress perpendicular to weld direction.

Figure 9 Plot of crack growth rate da/dN vs stress intensity factor range ΔK, ESE(T) samples at R = 0.1 and 0.6; FSW 2195-T8 Al-Li; crack plane perpendicular to the weld line.

Figure 10(a) Crack growth rate da/dN vs stress intensity range ΔK for three different sizes of ESE(T) samples at R=0.6; crack plane perpendicular to weld line.
Figure 10(b) Crack growth rate vs. crack length from the weld line for the three sizes of ESE(T) samples tested at R = 0.6; crack plane perpendicular to weld line. Shaded area shows position and extent of weld nugget and TMAZ.

Figure 11 Crack growth rate da/dN vs ΔK in three different sample sizes; C(T) samples crack plane parallel to the weld line.

Figure 12 Fracture surface of 185 mm x 50 mm ESE(T) sample; (1) Notch root; (2) parent material; (3) TMAZ; (4) weld nugget.

Figure 13 Comparison of fatigue crack fracture surface in (a) parent material, (b) welded C(T) with crack growing parallel to the weld line.

Figure 14 Crack deviation in 125 mm x 120 mm C(T) sample.

Figure 15 Effect of sample size on peak residual stresses; data points are maximum values of tensile residual stress parallel to weld line achieved in each sample geometry; represented on plot of weld length vs sample width.

Figures

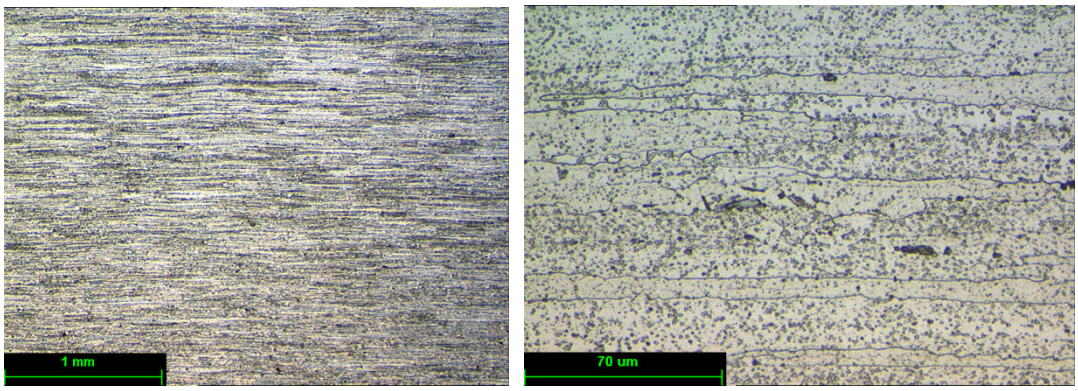

(a) (b)

Fig.1 a & b Microstructure of parent material 2195-T8 Al-Li alloy L-ST plane

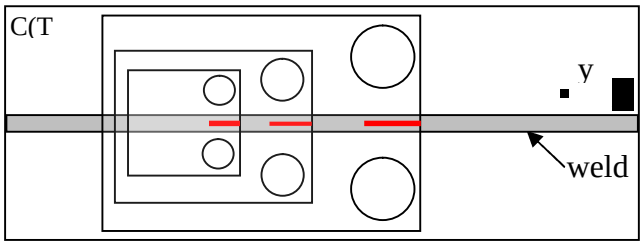

(a) C(T)

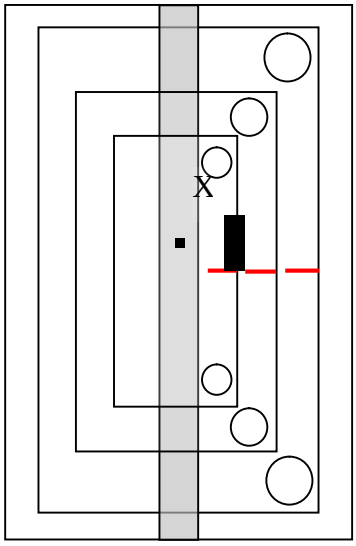

(b) ESE(T)

Fig.2 Schematic diagram showing weld location in (a) C(T) and (b) ESE(T) samples

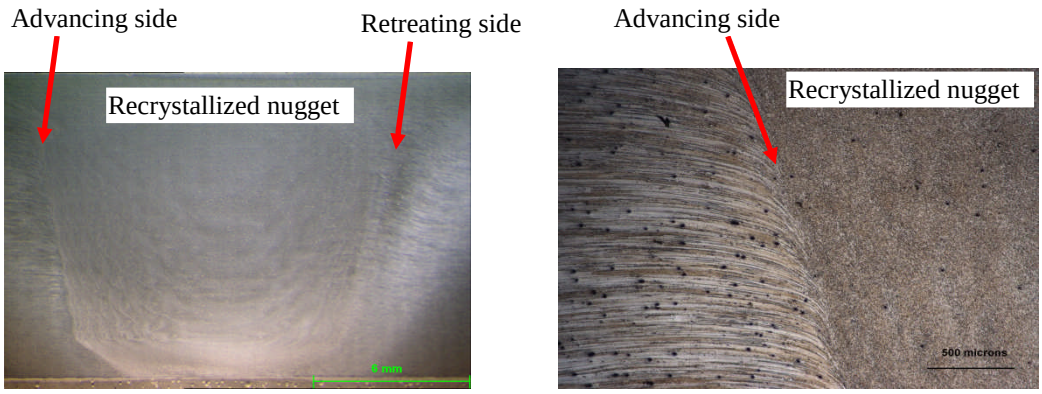

(a) Cross section view of weld (b) Microstructure in higher magnification

Fig.3 Macro and microstructure of weld zone in 2195-T8 FSW joints

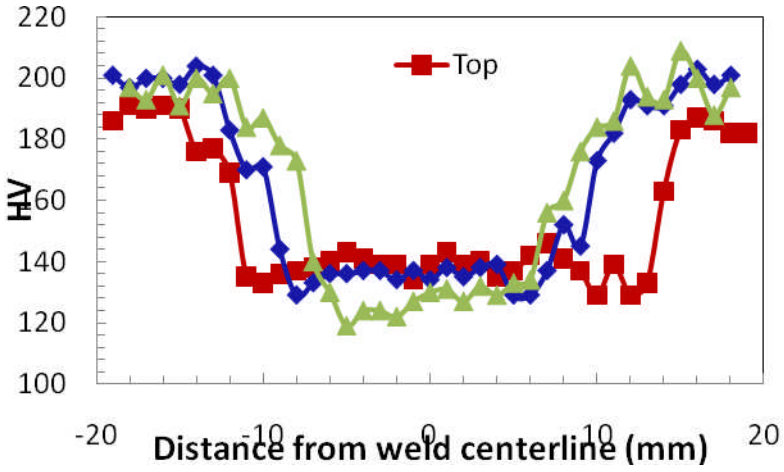

Fig.4 Vickers microhardness profiles of friction stir weld at top, bottom and mid-thickness sections across the weld

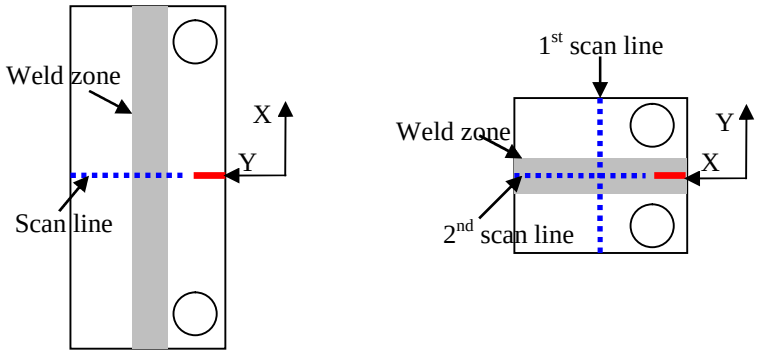

(a) ESE(T) (b) C(T)

Fig.5 ESET and CT samples showing scan lines for measurement of residual stress (a) ESE(T); (b) C(T)

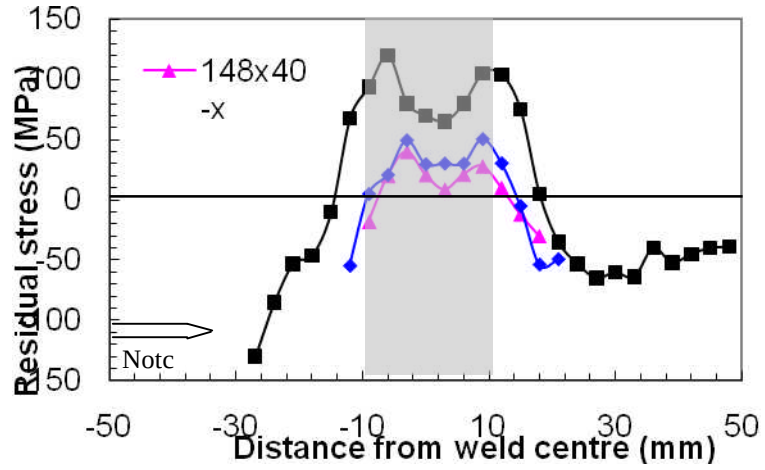

(a) Residual stress parallel to weld direction for 3 sizes of ESET samples

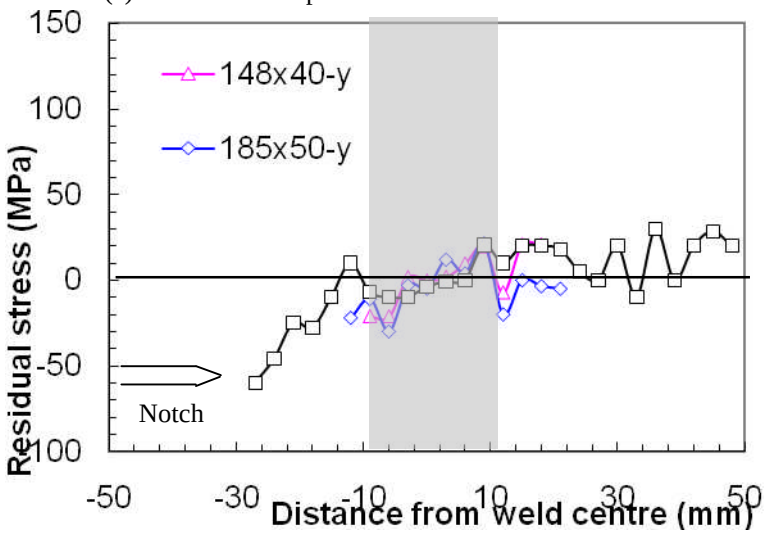

(b) Residual stress perpendicular to weld direction in 3 sizes of ESET samples

Fig.6 Residual stress profiles in ESE(T) samples

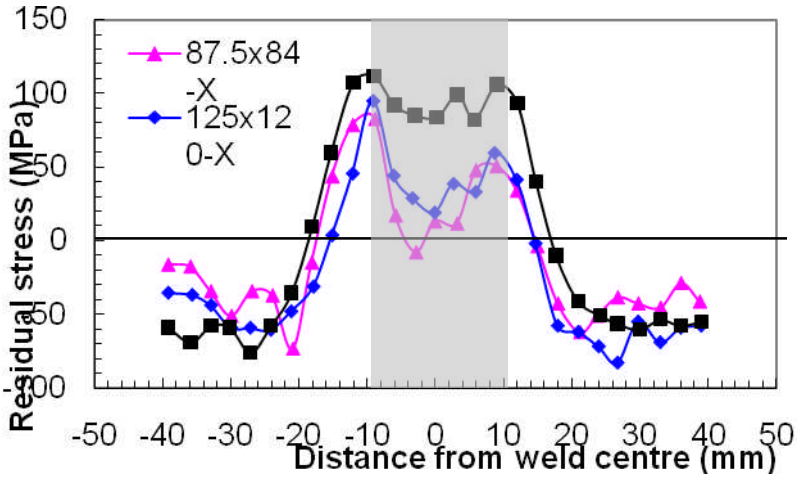

(a) Residual stress parallel to weld direction in 3 sample sizes (1st scan line)

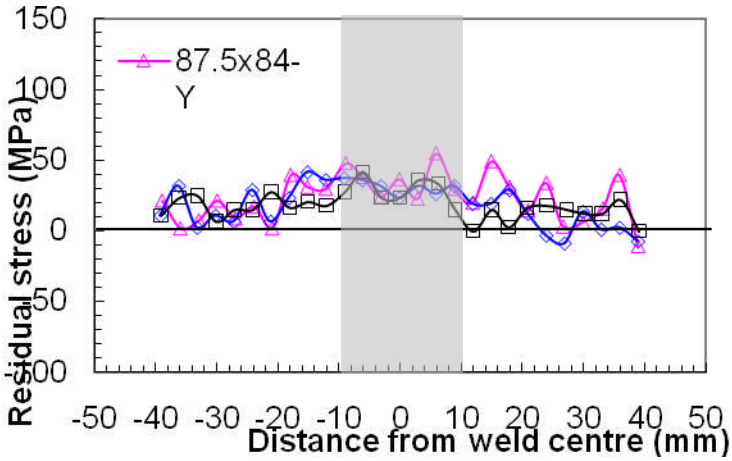

(b) Residual stress perpendicular to weld direction (1st scan line)

Fig.7 Residual stress profiles cross the weld (1st scan line) in three sizes of C(T) samples

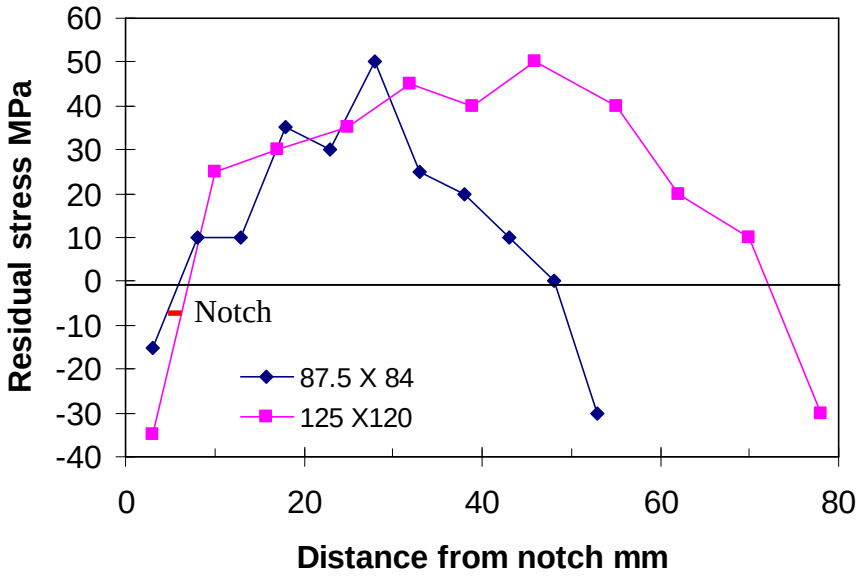

(a) Residual stress parallel to weld direction;

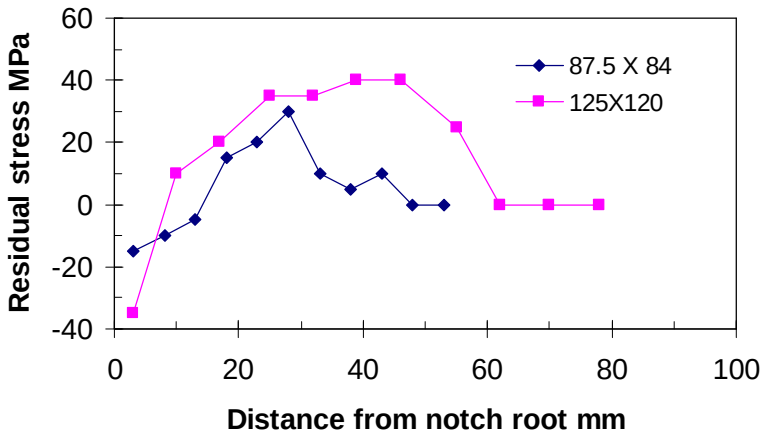

(b) Residual stress perpendicular to weld direction

Fig. 8 Residual stress changes along the weld line across the sample width, for the two smallest CT samples (2^{nd} scan line)

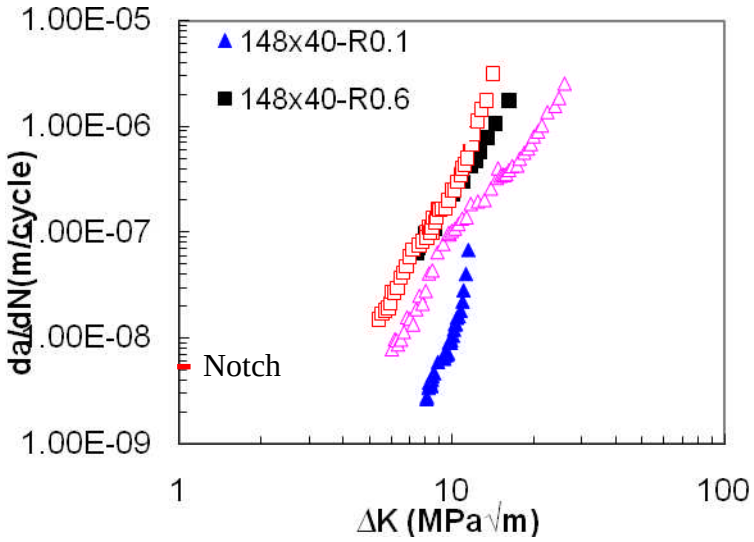

Fig.9 Plot of crack growth rate Vs stress intensity factor range ΔK , ESE(T) samples at R = 0.1 and 0.6; 2195-T8 Al-Li FSW crack plane perpendicular to the weld line.

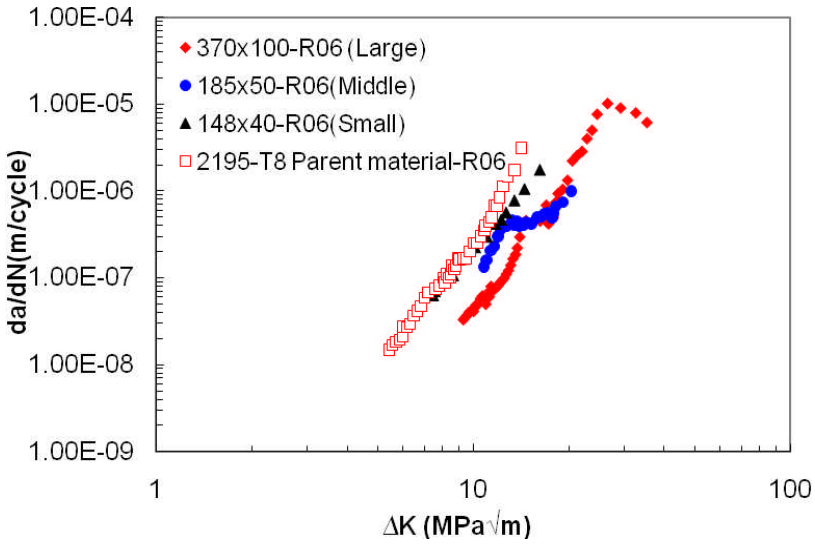

Fig.10a Crack growth rate da/dN Vs stress intensity range ΔK for three different sizes of ESE(T) samples at R=0.6; crack plane perpendicular to weld line

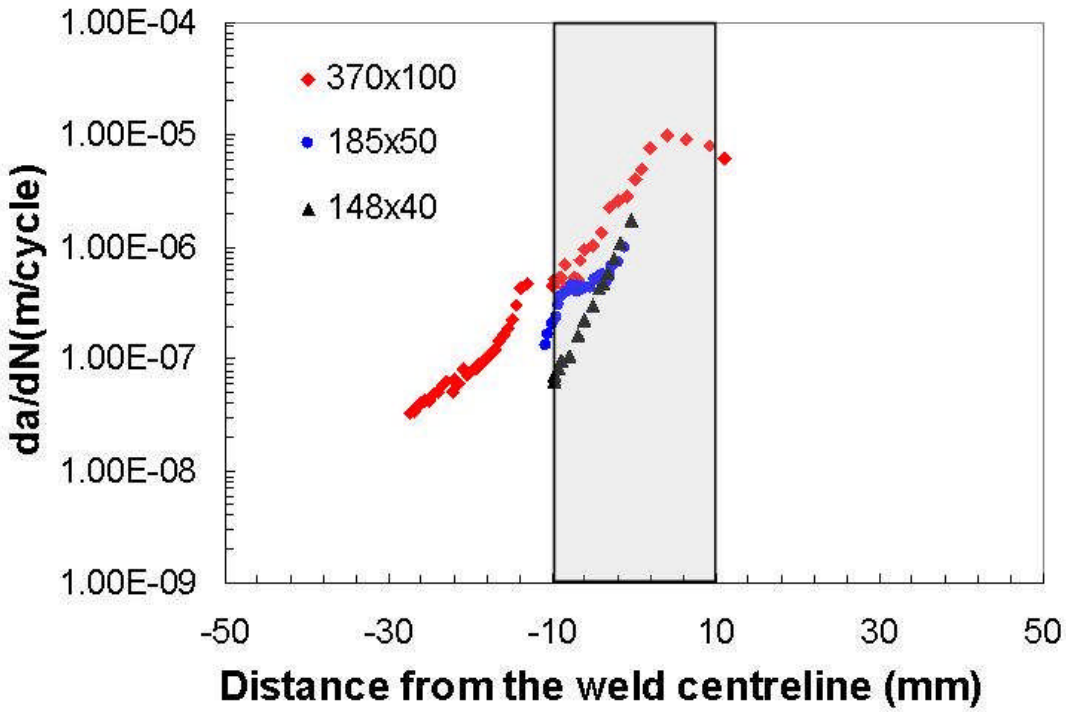

Fig 10b crack growth rate da/dN vs. distance from the weld centreline for 3 different sizes of ESET samples at R= 0.6; crack plane perpendicular to the weld line. Shaded area shows limits of nugget region

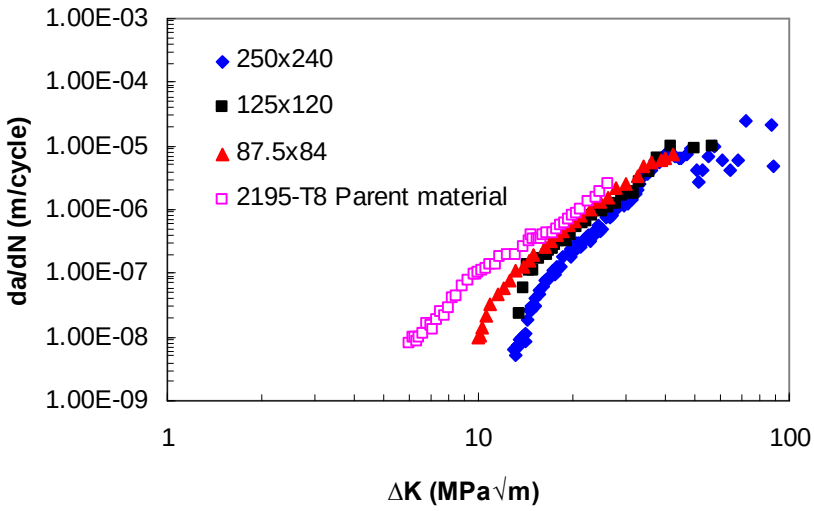

Fig.11 Crack growth rate da/dN Vs ΔK in three different sample sizes; C(T) samples crack plane along the weld line.

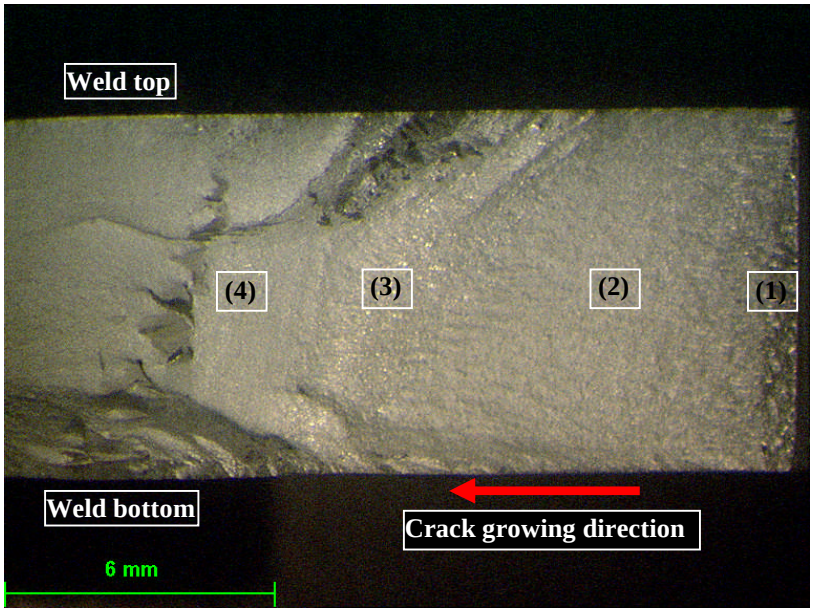

Fig 12 Fracture surface of 185 mm x 50 mm ESET sample
(1) Notch root; (2) Parent material; (3) TMAZ; (4) Weld nugget

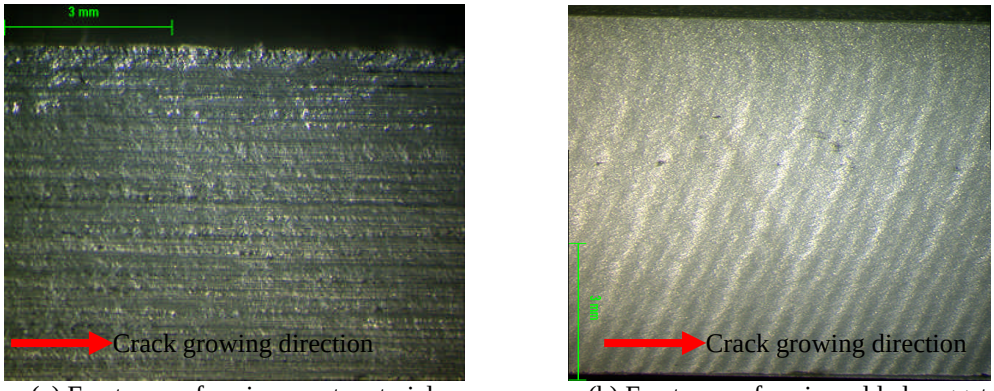

(a) Fracture surface in parent material (b) Fracture surface in welded nugget

Fig 13 Comparison of fatigue crack fracture surface in (a) parent material, (b) welded C(T) with rqack growing along the weld line

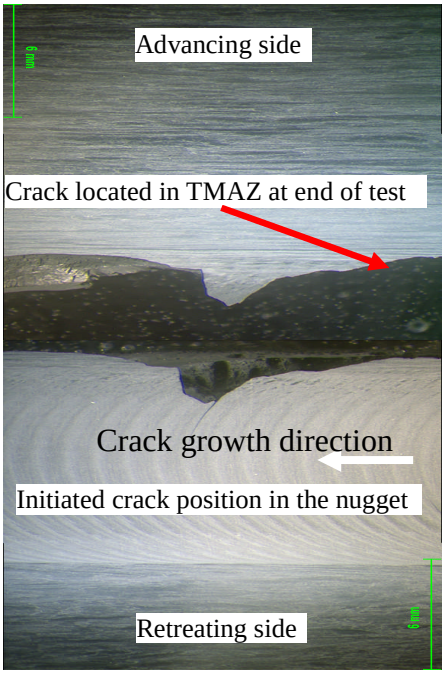

Fig.14 Crack location in TMAZ prior to final failure in 125 mm x120 mm CT sample

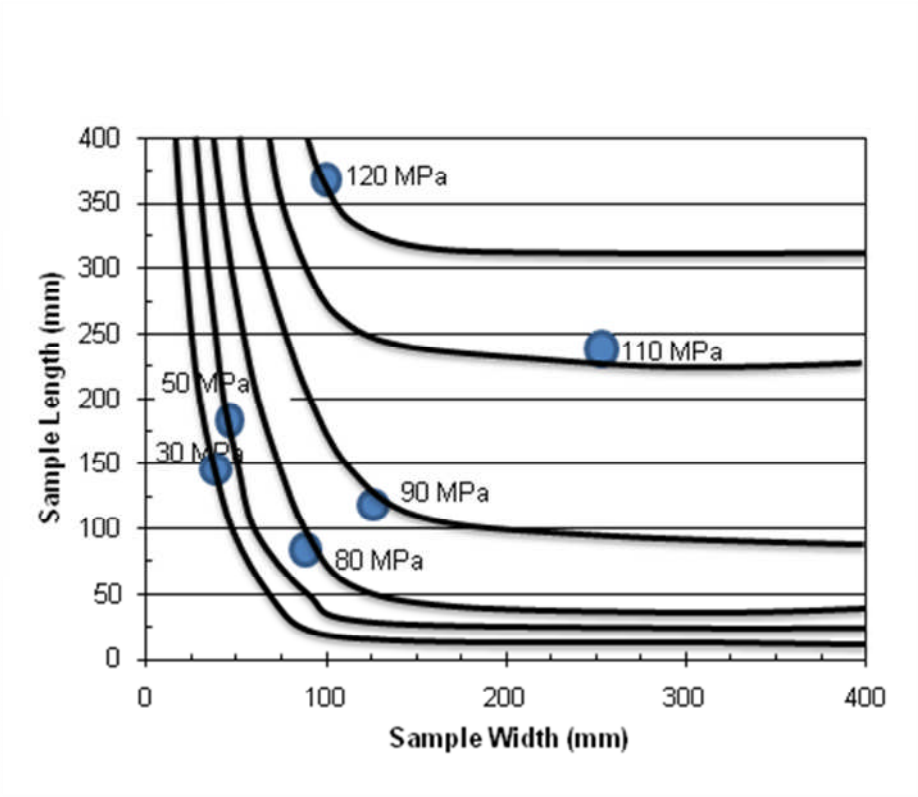

Figure 15 Effect of sample size on peak residual stresses; Data points are maximum values of tensile residual stress parallel to weld line achieved in each sample geometry; represented on plot of weld length Vs sample width. Estimated positions are shown of contours of equal residual stress consistent with measured data points and constraints of zero residual stress along axes.